Milli-Scale Biped Vibratory Water Strider *

Ki Yun Lee, Lu Wang, Jinhong Qu, and Kenn R. Oldham

Abstract— **This paper examines a centimeter-scale robot that relies on surface tension to move over a fluid, inspired by water strider insects. The millirobot in this work is 3D printed and actuated in vibrational resonance by an added piezoelectric strip. A simple empirical parametric analysis is performed, complemented by finite element modeling of robot structural vibration modes, to identify robot geometries producing motion over the water surface. Expanded results for the highest velocity robot iteration are presented, with some preliminary evaluation of general robot capabilities. This study is intended to help begin understanding how and why the robot moves in certain ways and give suggestions to future robot designs.**

Keywords—Microrobot, Bio-inspired Robot, Water Strider, Surface Tension, Piezoelectric, Rapid Prototyping

I. Introduction

Autonomous millimeter- and centimeter-scale robots have been proposed for applications ranging from the medical field to disaster management, but understanding the full range of locomotion possibilities for robots at these scales remains a subject of ongoing research. In recent years, several small-scale robots have been demonstrated that rely on surface tension to operate on a water surface, often inspired by the locomotion of water striders or other insects. Some prominent examples include the Miniature Water Strider Robot [1], Strider II [2], and Water Jumping Robot [3]. These robots used varying strategies to maintain reasonable power efficiency and load capacity. Suhr et al. [1] used Teflon® coated compliant legs to increase surface tension to ultimately increase load capacity. Detailed leg modeling was performed in [4, 5]. For Strider II descending from that work, Ozcan et al. [2] attempted to further increase load capacity by optimizing the number of feet and using multiple DC motors. This allowed Strider II to operate untethered. Yan et al. [3] designed a spatial cam mechanism to achieve complex movement of the robot such as jumping and rowing and utilized DC motors for high jumping height from the water. Jumping was also achieved primarily using surface tension in [6]. Other researchers have examined the use of hydrophilic [7] and partially submerged [8] leg-fluid interfaces to support robot weight.

In this work, robot development focuses on rapid prototyping and low power operation as motivated by prior work with terrestrial architectures for vibratory piezoelectric robots [9-11]. Resulting robots are 3D printed in polylactic acid (PLA), use a bipedal leg architecture, and are actuated by a piezoelectric lead-zirconate-titanate (PZT) strip. A typical model from this work has 18 mm diameter feet attached on either end of the 3 cm long PZT strip, for a total robot footprint of 10.4 cm^2. This results in a robot that is significantly smaller than its predecessors, as summarized in Table I. The robot generates either forward or lateral motion through vibratory coupling between its structure and underlying fluid at certain frequencies. Robot weight is 0.663 g (with body and PZT) with payload capacity up to 1.203 g.

This paper provides preliminary results on design, testing, and resulting locomotion of this class of milli-robot when utilizing vibratory excitation to move. Results are presented from a basic parametric analysis of robot foot and leg design features and locomotion trends as a function of voltage and excitation frequency.

TABLE I. Selected Examples of Surface Tension Enabled Robots

Source	Size (cm^2)	Number of Foot	Mass (g)	Transduction	Speed (mm/s)
Miniature Water Strider Robot [1]	16.0	4	0.67 (robot) 1.82 (load capacity)	Piezoelectric	23.0
Strider II [2]	166.3	12	21.75 (robot) 55 (load capacity)	DC Motor	71.5
Water Jumping Robot [3]	1575.0	6	5.50 (robot)	DC Motor	2420.7
This work	10.4	2	0.66 (robot) 1.20 (load capacity)	Piezoelectric	78.3 (unloaded)

II. Robot Design

Recently, Qu et al. demonstrated a small (~3 cm x 1 cm) bipedal robot driven by a single piezoelectric element adhered to a pair of cantilever-like leg and foot structures [10]. Through the selection of appropriate frequency and voltage inputs to the piezoelectric transducer, various gaits could be excited including hopping, walking, and running behaviors with reasonably large speeds, step heights, and efficiencies given the robot scale and low level of complexity.

These results inspired the authors to examine robot locomotion by similar means in other environments. Initial testing with thin platform-like feet attached to the original robot design showed the feasibility of locomotion on a fluid surface leading to empirical studies described in this paper.

Before studying basic parametric sensitivity, voltage and frequency trends, and load-bearing capacity, experiments to

*Research supported by the University of Michigan, the National Science Foundation, Award 1435222, and DARPA, award D18AP00071.

Ki Yun Lee, Lu Wang, Jinhong Qu, and Kenn R. Oldham are with the Department of Mechanical Engineering, University of Michigan, Ann Arbor, MI 48109, USA (corresponding author to provide phone: 734-615-6327; e-mail: oldham@umich.edu).

978-1-7281-0948-0/19/$31.00 ©2019 IEEE

determine a robot design that generates motion (referred to later as model 1) were conducted. Several design iterations were completed before identifying the basic structure of the biped "water striders" design shown in Fig. 1. A lead-zirconate-titanate (PZT) ceramic strip is adhered to a polymer frame to create a pair of symmetric legs with vertical struts at each end and a central flange to assist in balance. At the end of each strut, various foot structures can be attached to explore factors affecting robot locomotion.

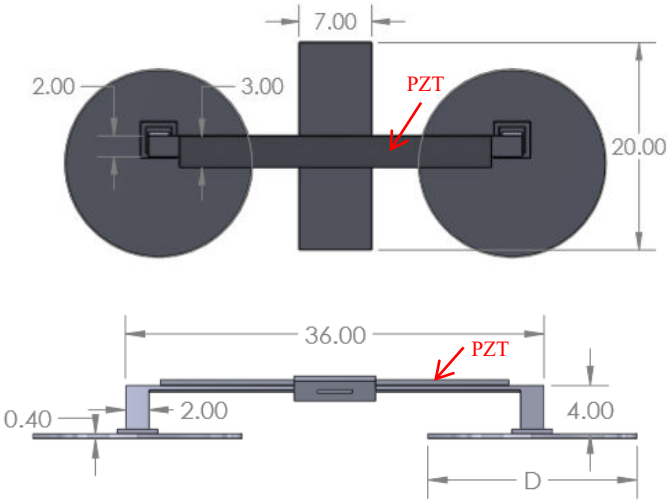

Figure 1. Top and front view of the water strider robot with dimensions. All dimensions in mm and hidden dimensions are the thickness of the body and angle of the body from the ground which is 0.4 mm and 5°, respectively. The diameter of feet, D is either 18 or 20 mm.

As shown in Fig. 1, the water strider robot is about 52 mm wide and 20 mm long. The robot's two feet are circular in shape so that there are no sharp lateral edges which tend to break the surface tension. The front and rear flange or "tail" aids in both balance and supporting the payload. A 3 mm x 30 mm x 0.45 mm PZT strip is mounted on top of the body with epoxy and an electric wire is connected to the top and bottom surfaces of the PZT to connect to a voltage source. Slack is provided as much as possible to minimize tension forces from the wire.

In the process of determining the robot design, features including weight, body thickness, the angle of the body, and location of feet were identified qualitatively as important factors in dictating whether locomotion would be generated. For example, initial robots featured four feet to have a bigger load-bearing capacity, but bipeds were ultimately chosen for further study because they were lighter and achieved much faster motion. In general, robot structure was printed as thin as possible (0.4 mm with current equipment) to maximize compliance with respect to the piezoelectric strip and reduce the weight of the robot, as long as the body and feet could sufficiently support external loads. The 5° angle of the body from the ground was chosen so that feet could apply thrust to the water at an angle while not being subject to "swamping" by water when supported by surface tension. Another important observation was that speed was much increased when struts were not connected to the center of the feet, but slightly off center so that the center of gravity of the robot is slightly forward.

Once a design that generated motion was achieved, a simple quantitative sensitivity analysis was conducted. In these studies, three main parameters were varied among a series of initial prototypes: foot diameter, offset of the center of the feet from the struts, and presence or absence of a rim on each foot to alter the stiffness and buoyancy behavior of the feet.

To identify resonant frequencies and begin interpreting propulsion by the feet, finite element modeling (FEM) was used. Modal analysis results in the air of the robot model are shown in Fig. 2. The first four vibration modes are displayed as computed by COMSOL Multiphysics software. In the first two vibration modes, Fig. 2(a) and 2(b), feet rotate in the y-direction but left and right foot rotate in opposite directions in mode 1 and in the same direction in mode 2. In the third and fourth vibration modes, Fig. 2(c) and 2(d), feet rotate in the x-direction, but likewise in opposite vs. shared directions mode 3 and mode 4, respectively. Due to the rotation of both feet in the same direction and the location of the center of gravity which makes the robot leans forward on the water, mode 4 (Fig. 2(d)) is anticipated to be most likely to produce net locomotion. Conceptually, the remaining modes displayed would not produce the net translation, though in practice we observed that mode 2 was also often associated with motion, lateral or sideways direction. This suggests to us that there is high sensitivity to (unintentional) manufacturing asymmetries when exciting this mode, as well. There are many higher-order modes that are not shown here, but they were not observed to generate locomotion.

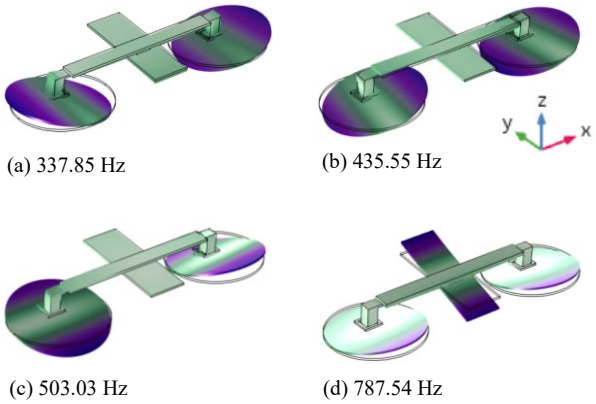

(a) 337.85 Hz (b) 435.55 Hz

(c) 503.03 Hz (d) 787.54 Hz

Figure 2. Vibration mode 1, 2, 3, and 4 at (a) 337.85 Hz, (b) 435.55 Hz, (c) 503.03 Hz, and (d) 787.54 Hz, respectively. Modes are analyzed by COMSOL Multiphysics software.

III. Experimental Setup

A. Robot Fabrication

The body and feet of the robot were manufactured using a 3D printer (PrintrBot) with infill 100% and layer height 0.2 mm. The printing material was polylactic acid (PLA). The body and feet were printed separately, then they were connected by commercial epoxy. After curing the epoxy, a PZT strip was glued on top of the body by the same epoxy. Then, single strand electrical wires were connected to the top and bottom of the PZT strip using silver epoxy.

B. Robot Testing

For experiments, a function generator (HP 33120A), amplifier (TEGAM Model: 2350S-020-2K, Serial Number: 0514008), high-speed camera (SONY DSC-RX10M3, Serial Number: 099811, 960fps), and plastic container were used. Before the experiments, a ruler sheet with 1cm x 1cm gridlines was added beneath the container to set the coordinate axis and to calibrate tracking software. The container was filled with water and camera clamped perpendicularly over the water surface so that we could directly calculate velocities. The range of voltage available for PZT driving was from 10 V to 100 V with the amplifier (20x) and the range of frequency tested was from 50 Hz to 1000 Hz, using sine wave excitation. For each experiment, a video was taken using the camera. To capture the frequency of ripples generated in the water, another video was taken using high-speed camera mode (960 fps). Tracking software Tracker (https://physlets.org/tracker/) was used to measure velocity during robot tests.

IV. Results

Initial testing of robots with varying foot geometries was used to identify the candidate design achieving maximum speed. Additional testing on this robot was then performed to more fully evaluate performance and acquire data for further analysis in future works.

A. Parametric Study

For the simple parametric study, three parameters were chosen and changed across experiments. The three parameters were the diameter of a foot (18 or 20 mm), offset of the center of the feet (3/8 of the diameter or center), and presence or absence of a rim on each foot. The directions of motion and speed of the robot based on these parameters are shown in Table II. For example, model 1 has 18 mm diameter feet and no rim on feet and the connection between the struct and feet is at off-center. Model 1 has the maximum forward and lateral speed at 730 and 425 Hz; corresponding natural frequencies for forward and lateral motion suggested by FEM were 787.54 and 435.55 Hz, respectively.

TABLE II. Results of Varying Foot Designs. Directions of motion, speeds, and frequencies when maximum speeds occurred are shown. Natural frequencies of vibration modes by COMSOL FEM are shown as well. N/A represents no motion. L and R represent motion in left and right, respectively.

Parameter	**Experiment (Hz)**				**COMSOL (Hz)**	
	Forward Motion ↕	***Speed (mm/s)***	***Lateral Motion*** ↔	***Speed (mm/s)***	***Forward Motion*** ↕	***Lateral Motion*** ↔
Model 1 18 mm Off-center No Rim	730	68.63	425	39.28	787.54	435.55
Model 2 20 mm Off-center No Rim	670	62.66	330	14.34	698.32	368.82
Model 3 18 mm Center No Rim	N/A	N/A	410, 770	16.07, 16.22	789.54	431.42
Model 4 18 mm Off-center Rim	N/A	N/A	360(L) 750(R)	11.75(L) 78.28(R)	789.86	373.02

Robot excitation was performed from 50 to 1000 Hz at 100 V for each of the four models. Typically, each model has two ranges of frequency which generate locomotion, a lower and higher frequency region. We observed that at the lower frequency region, the robots moved in the lateral direction, while the higher frequency region is associated with forward motion. Each frequency range varies in width based on model type, but usually covered about 100 Hz and no locomotion was generated outside of those ranges. A specific frequency when the maximum speed occurred within each range of frequency were measured by Tracker software. A FEM model was built COMSOL to analyze the direction of motion for each model, for which natural frequencies of vibration modes with shapes resembling mode 2 and mode 4 in Fig. 2(b) and Fig. 2(d) are shown in Table II as well.

Most results show that motions happened near frequencies associated with characteristic mode shapes noted above are predicted in COMSOL. In particular, for lateral motion of all four models and forward motion of the first two models, maximum speed was achieved slightly below the frequency of coordinated foot rotation in the associated directions. This suggests to us that there is an only mild impact of fluid inertial loading and damping on the modal frequencies of these robots and that net forcing is achieved by some coupling of vibration with the fluid interface aided by asymmetry. Indeed, when forward asymmetry is removed (model 3), no forward motion is not observed.

However, there are some unexpected experimental results. In particular, both models 3 and 4 achieve lateral motions at frequencies (770 and 750 Hz) not associated with mode shapes that would seem to suggest motion. In addition, it is not clear how directionality of lateral motion is determined, lacking center of gravity bias present for forward motion. For example, model 4 moved to the right at 750 Hz while all other models translated to the left. Model 4 also achieved forward locomotion at a higher frequency than its nominal modal frequency, unlike other scenarios producing motion. Whether these results are due to imperfections in robot fabrication or experimental test perturbations (i.e. from the wire tether) and/or some unmodeled interactions between structural and fluid dynamics remains to be studied.

B. Voltage and Frequency Trends

Locomotion speed was then assessed across varying voltage and frequency inputs for model 1 (the representative model which has 18 mm feet, offset of the center of the feet, and no rim on the feet). Images of this model moving forward and to the left are shown in Fig 3. These images are extracted from videos that we took for this experiment. In Fig. 3(a), the robot was moving forward and the velocity was 68.63 mm/s, which is about 3.5 times the body length. In Fig. 3(b), the robot was moving to the left and the velocity was 39.28 mm/s which is about two times the body length.

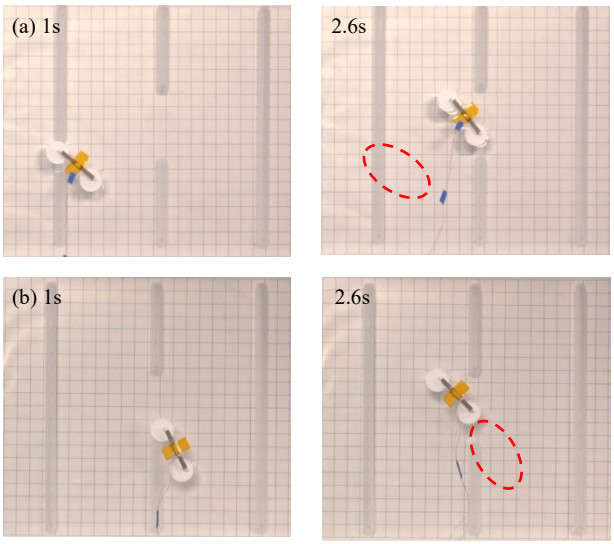

Figure 3. (a) Forward motion at 730 Hz, 100 V from 1 to 2.6 s; (b) lateral motion at 425 Hz, 100 V from 1 to 2.6 s. Red markers represent the previous position of the robot. The grid in the background has a size of 1 cm x 1 cm.

For this voltage and frequency trends, the voltage was varied from 60 to 100 V over 20 V increments and frequency was varied from 700 to 800 Hz over 10 Hz increments. Once experiments were complete, velocities were calculated by Tracker and data compiled in MATLAB. In order to find the speed of the robot at each experiment, we picked the speed calculated from total speeds when the speed reaches a plateau and becomes steady. It should be noted that motion was produced against some small tension in the wire tether, such that when power was removed, the robot would return to its original position. The voltage and frequency trends are shown in Fig. 4.

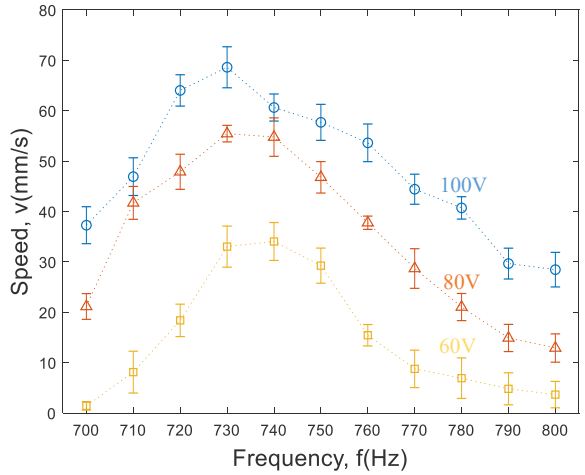

Figure 4. Voltage and frequency trends. Voltage and frequency varied from 60 to 100 V and 700 to 800 Hz, respectively.

In Fig. 4, when the voltage increased, the speed of the robot increased at any frequency within the range, such that the trend between speed and voltage is approximately proportional. For the frequency trend, generally, the magnitude of velocity decreases as frequency moves away from the natural frequency of the robot in the air, suggesting that structural resonance is a critical factor in producing locomotion. Only a mild reduction in maximum frequency was observed with increasing motion amplitude; the maximum speed of robot model 1 at 60, 80, and 100 V occurred at 740, 730, and 730 Hz. It should be noted that since Tracker cannot track perfectly without missing exact locations of the robot, the speed at each data point was calculated by the average of speeds across several image frames among each data point when the speeds reach a plateau. The error bars in Fig. 4 was generated from one standard deviation of the speeds captured across image frames.

C. *Load-bearing Capacity*

While active robot testing was performed using wire tethers without additional mass, separate experiments were done to measure the amount of load that could be carried before the robot capsized. The brief procedure of the experiment is the following. While the robot is on the water, external masses were added on the robot to figure out how much weight the robot can carry. The result is that the robot can carry up to 1.203 g. Regarding this external mass, the robot with a PZT strip can carry about two times the weight of the robot and the PZT.

During the experiment, the position of the external mass was found to be an important factor to affect the load-bearing capacity. If the external masses is placed at the center of the robot and the weight of the mass exceeds the limit, the robot sinks vertically since surface tension cannot overcome the weight of the mass. On the other hand, if external masses were added onto either front or rear tail, the robot will tip over and capsize at much lower load limit. The limitation of load-bearing capacity varied among models. For example, model 2 and 4, despite having either larger (20 mm vs. 18 mm diameter) feet or a rim on the feet, respectively, could carry less additional payload because the initial robot mass was larger. The largest added payload was achieved for the robot with the smallest initial mass which is model 1. Model 1's payload capacity was 1.20 g, compared to a 0.66 g body and PZT mass.

D. *Discussion*

Evaluation of the robot presented in this work is largely empirical, and at this time the robot does not offer obvious practical applications. However, the robot has intriguing performance characteristics and may provide further concepts for producing useful structural-fluidic interactions in robotic or small-scale applications.

One common advantage of small piezoelectric actuators is small power consumption. With a capacitance of approximately 6 nF, power consumption at maximum speed is 21 mW, while forward motion can be initiated at less than 900 μW. This results in respectable cost-of-transport characteristics, measured as P/mgv, where m is robot mass, g is gravitational constant, v is robot speed, and P is input power. For the unloaded robot, cost of transport at maximum speed is approximately 40, which is on the same order of magnitude as that of terrestrial animals of comparable mass, though large relative to swimming organisms [12].

Relatively efficient coupling of robot vibration to forward locomotion appears to depend on the existence of compliance and asymmetry in robot feet. Due to the angle of the body and

offset of the feet, the robot can provide some apparent thrust to water, despite the small size. In addition, the center of gravity of the robot is located forward of the midline of the feet so that the front edges of the feet sink slightly. These features are easy to visually observe. In terms of models, model 1 is the best design to date for producing forward motion. Larger feet (model 2) reduce speeds in forward motion due to either increased weight or drag. Struts at the center of feet (model 3) produce less effective thrust into the water and a rim on feet (model 4) seems to hinder the robot from moving forward.

The lateral motion was unexpected because the robot designs lacked asymmetry in the lateral direction. However, since we observed the robot moved in the lateral direction, we believed unintentional imbalance produces net motion at lateral modes. In separate experiments using Laser Doppler Vibrometer (LDV) and a scanning XZ laser profile sensor, amplitudes of vibration of the left and right foot at the same frequency were different. In addition, several unexpected experimental outcomes were arisen for lateral motion, noted in Section IV. A. Some factors that might be associated with these situations include that wire tension might affect the direction. The robot was tethered and it was found that the magnitude of tension force by wires was nonzero. We observed that when speed was low (around 10 mm/s), the robot did not fully overcome the tension. Thus, directionality at low speeds might be affected by tension. Second, since the robot was 3D printed, density was not distributed equally among robots or on the left and right side of the body. Lastly, since the robot was light, the weight of epoxy might further perturb the system. The epoxy was not distributed on a PZT equally, so the weight distribution of the robot again is not fully symmetric.

Interestingly, the coupling between structural motion and fluid also appeared to take place at disparate time scales. While excitation frequencies that produce motions for model 1 occurred near 400 Hz and 700 Hz for model 1, ripples or waves generated in the water were observed at much lower frequencies and with longer characteristic lengths. The image of ripples generated at 425 Hz and 100 V is shown in Fig. 5.

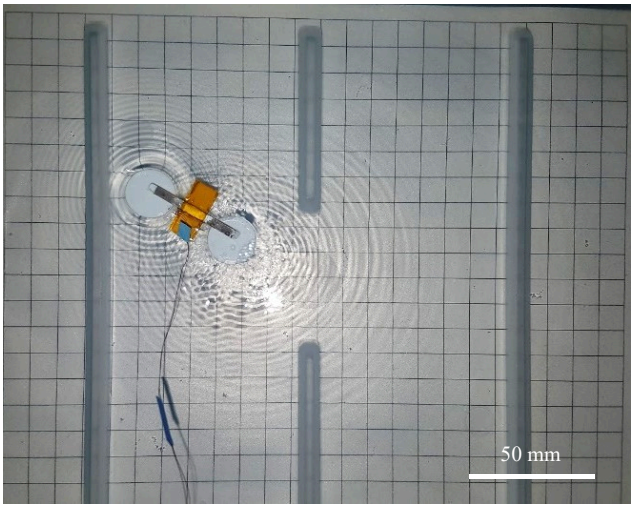

Figure 5. Ripples generated at 425 Hz and 100 V by model 1. This was when the robot was moving left. Also, we can clearly see that ripples generated by the right foot were more than by the left foot and this behavior caused the robot moved to the left.

The motion of the robot at 425 Hz and 100 V were taken by a high-speed camera (960 fps) and all frames were extracted from the video to measure the frequency of ripples. We roughly estimated how many ripples were generated over a second and found the frequency of the ripples is about 19 Hz. Therefore, the coupling between the structure and fluid generates a ripple frequency different from excitation frequency.

The above observations suggest that there is a wide design space remaining to explore and potentially interesting features of the design can be extracted from a more fundamental analysis of structural/fluid mechanics of the system.

V. Conclusions

A water strider-inspired centimeter-scale using vibratory leg excitation was examined through preliminary modeling and experimental studies. From experimental observation, first, most models typically have forward and lateral motion at two different ranges of frequencies. Second, maximum speeds of forward motion are much higher than maximum speeds of lateral motion in most cases. Among all four models, the maximum speed achieved for a forward and lateral motion was 68.63 mm/s by model 1 and 78.28 mm/s by model 4. There is an approximately proportional relationship between speed and voltage, while high velocity operating frequency appears to be associated with certain characteristic mode shapes of robot structural vibration in the absence of a fluid interface.

The ranges of frequencies and directions of motion that were observed for each model and in finite element modeling suggests some interpretations as to which frequency the robots will move at and why it moves in a certain direction. However, even if this FEM model gave some insight, further study is needed to fully understand the motion of the robot especially when coupled with the underlying fluid. For example, according to FEM, there is a mode that represents rotational motion and we have not observed this motion. Planned further study includes simulation of the robot in multiphase flow. Such simulation is hoped to demonstrate how the flow is generated by feet while moving. Furthermore, given this flow simulation, multiple vibration modes, and parametric tests, we would like to achieve effective control of the robot and predict speeds as a function of frequency for better performance.

Acknowledgment

The robot models were fabricated in UM3D Lab and all the experiments were performed in Microdynamics Laboratory: Microsystems at the University of Michigan.

References

[1] S. H. Suhr, Y. S. Song, S. J. Lee, and M. Sitti, “Biologically Inspired Miniature Water Strider Robot,” Proceedings of the Robotics: Science and Systems I, pp. 319-325, 2005.

[2] Ozcan, Onur, Han Wang, Jonathan D. Taylor, and Metin Sitti. “STRIDE II: A Water Strider-Inspired Miniature Robot with Circular Footpads.” International Journal of Advanced Robotic Systems, (June 2014). doi:10.5772/58701.

[3] J. Yan, T. Wang, X. Zhang and J. Zhao, "Structural design and dynamic analysis of biologically inspired water-jumping robot," 2014 IEEE International Conference on Information and Automation (ICIA), Hailar, 2014, pp. 1295-1299. doi: 10.1109/ICInfA.2014.6932848

[4] Y.S. Song, M. Sitti, "Surface-tension-driven biologically inspired water strider robots: Theory and experiments," IEEE Transactions on Robotics, Vol. 23, No. 3, pp. 578-589, 2007.
[5] Y.S. Song, S.H. Suhr, M. Sitti, "Modeling of the supporting legs for designing biomimetic water strider robots," IEEE International Conference on Robotics and Automation, Orlando, FL, May 2006.
[6] J.-E. Koh, E. Yang, G.-W. Pil, S.-P. Jung, J.H. Son, S.-I. Lee, P.G. Jablonski, R.J.Wood, H.-Y. Kim, and K.-J. Cho, "Jumping on water: surface tension-dominated jumping of water striders and robotic insects," Science, vol. 349, no. 6247, pp. 517-521, Jul 2015.
[7] K. Suzuki, H. Takanobu, K. Noya, H. Koike, H. Miura, "Water strider robots with microfabricated hydrophobic legs," IEEE/RSJ International Conference on Intelligent Robots and Systems, San Diego, CA, Dec 2007.
[8] X. Zhang, J. Zhao, Q. Zhu, N. Chen, M. Zhang, and Q. Pan, "Bioinspired aquatic microrobot capable of walking on water surface like a water strider," ACS Applied Materials and Interfaces, vol. 3, no. 7, pp. 2630-2636, Jun 2011.
[9] J. Qu, C.B. Teeple, and K.R. Oldham, "Modeling legged microrobot locomotion based on contact dynamics and vibration in multiple modes and axes." Journal of Vibration and Acoustics, vol. 139, no. 3, pp. 031013, Apr 2017.
[10] J. Qu, B. Zhang, and K.R. Oldham, "Design and analysis of varied gaits in elastic vibratory milli-robots," International Journal of Intelligent Robotics and Applications, vol. 2, no. 4, pp. 400-412, Dec 2018.
[11] K. Patel, J. Qu, K.R. Oldham, "Tilted leg design for a rapid-prototyped low-voltage piezoelectric running robot," International Conference on Manipulation, Automation, and Robotics at Small-Scales, Nagoya, Japan, Jul 2018.
[12] V.A. Tucker, "The energetic cost of moving about," American Scientist, vol. 63, no. 4, pp. 413-419, Jul-Aug 1975.